Conf-911213--19

THE EFFECT OF PROCESSING PARAMETERS DURING HEAT TREATMENT OF BULK HIGH-T_c SUPERCONDUCTORS*

Y. S. Cha, S. E. Dorris, J. R. Hull, and R. B. Poeppel

Materials and Components Technology Division
Argonne National Laboratory
Argonne, IL 60439

Approved by OSTI

ANL/CP--72939

DE92 004149

April 1991

The submitted manuscript has been authored by a contractor of the U. S. Government under contract No. W-31-109-ENG-38. Accordingly, the U. S. Government retains a nonexclusive, royalty-free license to publish or reproduce the published form of this contribution, or allow others to do so, for U. S. Government purposes.

DISCLAIMER

This report was prepared as an account of work sponsored by an agency of the United States Government. Neither the United States Government nor any agency thereof, nor any of their employees, makes any warranty, express or implied, or assumes any legal liability or responsibility for the accuracy, completeness, or usefulness of any information, apparatus, product, or process disclosed, or represents that its use would not infringe privately owned rights. Reference herein to any specific commercial product, process, or service by trade name, trademark, manufacturer, or otherwise does not necessarily constitute or imply its endorsement, recommendation, or favoring by the United States Government or any agency thereof. The views and opinions of authors expressed herein do not necessarily state or reflect those of the United States Government or any agency thereof.

To be submitted for presentation at the 1991 ASME Winter Annual Meeting, Session on "Bulk Processing and Mechanical Properties of High-T_c Superconductors," Atlanta, GA, December 1-6, 1991.

*Work was supported by the U.S. Department of Energy, Conservation and Renewable Energy, as part of a program to develop electric power technology, under Contract W-31-109-Eng-38.

MASTER

DISTRIBUTION OF THIS DOCUMENT IS UNLIMITED

THE EFFECT OF PROCESSING PARAMETERS DURING HEAT TREATMENT OF BULK HIGH-T_c SUPERCONDUCTORS

Y. S. Cha, S. E. Dorris, J. R. Hull, and R. B. Poeppel

Materials and Components Technology Division
Argonne National Laboratory
Argonne, IL 60439

Abstract

Plastic extrusion is a promising method for producing the long lengths of high-T_c superconductor that will be necessary to meet many potential applications. A crucial phase of the extrusion method is removal of organic constituents. Incomplete removal can leave residual carbon at grain boundaries, which can adversely affect the superconducting properties, whereas excessively rapid removal of the organics can cause the extruded superconductor to disintegrate completely. In this paper, we analyze the effects of the following aspects of organics removal, as they apply to the firing of extruded $YBa_2Cu_3O_x$ coils: (a) total pressure in the furnace, (b) oxygen flow, (c) heat conduction, and (d) diffusion of volatile components during removal of organics.

Introduction

For many practical applications of high-T_c superconductors, it will be necessary to make long, continuous lengths of superconductor in a variety of shapes. Thin-film techniques have produced the best-performing superconductors to date, with critical current densities on the order of $\approx 10^6$ A/cm^2 [1]. However, such techniques are limited to production of

superconductors for small-scale applications. Large-scale applications will require bulk fabrication processes such as plastic extrusion, a versatile technique that has been used to produce long lengths of continuous $YBa_2Cu_3O_{7-x}$ (YBCO) superconductor in the form of multilayer coils.

In the green state, extruded superconducting coils contain ≈10 wt% organics. These organics perform important functions in the extrusion process. For example, they prevent agglomeration of the YBCO during milling, and they provide the green coil with strength and flexibility. However, before the green coil can be made into a useful superconductor, the organics must be completely and carefully removed.

The removal of organics is a complicated process involving a delicate balance between heat and mass transfer through a structurally weak body. Heat must be conducted into the coil interior to maintain thermal equilibrium and initiate decomposition of the organic phase. Volatile species formed at low temperatures ($T<240°C$) must diffuse to the surface rapidly enough to avoid formation of bubbles in the interior. At higher temperatures ($T\geq260°C$), decomposition of the binder proceeds by either thermal unzipping or oxidation. In the case of thermal unzipping, the monomeric species must diffuse rapidly to the surface to avoid bubble formation. For oxidation, oxygen must diffuse to the interior where it can react with the binder, and the products of this reaction must diffuse to the surface where they can be removed. In either case, heat generated by decomposition of the binder must be removed by conduction to prevent thermal runaway at the sample interior. In addition to the above considerations, relatively large amounts of CO_2 and H_2O are generated during the removal of organics, and it has been shown that CO_2 and H_2O

severely affect the transition temperature, critical current density, and superconducting transition width of YBCO superconductors [2–7]. To better understand and control these processes during the heat treatment of YBCO coils, the effects of the following factors were analyzed: (a) total pressure in the furnace, (b) oxygen flow, (c) heat conduction, and (d) diffusion of volatile components during binder removal.

Experimental

Powders of YBCO and Y_2BaCuO_5 (211) were made by solid–state reaction of the constituent oxides. To prepare for extrusion, YBCO powder was first mixed with a solvent, a dispersant, a binder, and a plasticizer; it was then mixed with silver. This yielded a plastic mass that was first extruded, then coated with 211, to give an insulated YBCO/Ag wire that could be wound into a coil. The addition of silver improved the mechanical properties of the fired wire. Superconductor wires with diameters between 0.1 and 3.0 mm and lengths up to 20 m have been extruded at Argonne National Laboratory. After extrusion, coils are fired at 900–920°C in flowing oxygen (1160 cm^3/min) at a reduced total pressure (≈2 torr), then annealed in 100% oxygen for up to 48 h at 450°C. The critical current density, J_c, of coils was measured by the four–probe technique, with a criterion of 1 μV/cm. Details on the fabrication procedure are given elsewhere [8].

Results and Discussion

Table 1 shows the firing conditions for six coils made by extrusion, their critical current densities, J_c, and the magnetic field generated at the center of the coil when the coil was operating just below its critical current. Also shown, for two coils, are the magnetic fields generated across the

6-mm gap of an iron core. Although the J_c values are well below those necessary for applications such as electric motors, the length of continuous superconductor ranges up to ≈20 m in these coils. Moreover, the measurements were made in magnetic fields up to 73 G, and fringing effects at the coil ends probably increase the field on the end winding even further. The J_c values are typical of bulk YBCO produced by conventional ceramic processing methods, i.e., they still appear to be controlled by weak links; however, the long lengths represent a significant improvement in the fabrication of bulk superconductors. In particular, the results indicate that the process of organic removal has been successfully controlled.

Total Pressure in Furnace. When superconducting coils are fired at ambient pressure, harmful concentrations of CO_2, CO, and H_2O accumulate in the atmosphere, leading to gross decomposition of YBCO. By contrast, their concentrations are minimized when the coils are fired at a reduced total pressure, and decomposition of YBCO is greatly reduced, if not completely avoided. Also, the binder decomposition reaction can be moderated somewhat by reducing the concentration of oxygen available for oxidation of the binder.

The effect of total pressure is demonstrated in Fig. 1 and 2, which show schematic X-ray patterns of two YBCO powders that were mixed with the organics used in extrusion, then heated in flowing oxygen at either ambient (Fig. 1) or reduced (Fig. 2) pressure (≈2 torr). Samples were taken from the mixtures at 240, 300, and 350°C, and their X-ray patterns were obtained. Figure 1 shows that, when YBCO/organic mixtures were fired at ambient pressure, both samples of YBCO decomposed (powder prepared by the liquid-mix process decomposed at 240°C, whereas that prepared by solid-

state reaction decomposed at 300°C). However, Fig. 2, which shows that the relative intensities of peaks varied with temperature, also shows that YBCO powders heated at reduced pressure did not decompose.

The patterns at 240 and 350°C indicate highly oxygenated YBCO, whereas the pattern at 300°C indicates oxygen-deficient YBCO [9]. This is consistent with measurements that showed a weight gain between 300 and 350°C and suggests that, as the organics are oxidized in the temperature range of 240–300°C, they remove oxygen from the YBCO. Once the organics have been completely removed (above ≈300°C), YBCO regains the lost oxygen and shows an increase in weight. These results indicate that firing at reduced total pressure prevents gross decomposition of YBCO. Therefore, firing at reduced total pressures is important to the fabrication of multilayer coils.

Effect of Oxygen Flow. The furnace used to fire coils is diagrammed in Fig. 3. The vacuum pump maintains a reduced pressure in the furnace and minimizes decomposition of YBCO, as discussed above. A throttle valve is placed between the oxygen flowmeter and the furnace to keep the exit end of the flowmeter at ambient pressure. This is done so oxygen flow can be measured with a flowmeter that was calibrated at ambient pressure. Downstream from the throttle valve, the oxygen flow begins to accelerate and its velocity becomes quite high when it reaches the furnace. The velocity of the oxygen flow at the entrance to the furnace depends primarily on the pressure ratio, P_2/P_1, i.e., on the pressure at the entrance to the furnace/the pressure just downstream from the throttle valve.

In analyzing the effect of P_2/P_1 on the gas velocity, temperature, and density, we assume that the flow between Points 1 and 2 (Fig. 3) is one-dimensional and adiabatic. This leads to the following equations, which apply to the flow of a perfect gas through a constant area [10]:

$$P_2/P_1 = (M_1/M_2)\,(A_2/A_1)^{1/2}, \tag{1}$$

$$T_2/T_1 = A_2/A_1, \tag{2}$$

$$V_2/V_1 = (M_2/M_1)\,(A_2/A_1)^{1/2}, \tag{3}$$

and

$$\rho_2/\rho_1 = (M_1/M_2)\,(A_1/A_2)^{1/2}, \tag{4}$$

where

$$A = \frac{\gamma+1}{2\left(1+\frac{\gamma-1}{2}M^2\right)}, \tag{5}$$

γ is the specific heat ratio ($\gamma = 1.395$ for oxygen), and M is the Mach number. The upstream conditions at Point 1 are known, and in the present analysis, we assume $T_1 = 26°C$, and $V_1 = 1$ m/s. These conditions yield

$$C_1 = (\gamma RT)^{1/2} = [(1.395)(260)(299)]^{1/2} = 330 \text{ m/s}, \tag{6}$$

$$M_1 = V_1/C_1 = .0/330 = 0.0030, \tag{7}$$

and

$$A_1 = \frac{\gamma+1}{2\left(1+\frac{\gamma-1}{2}M_1^2\right)} = 1.197. \tag{8}$$

Equations (1)-(4) can be expressed in terms of the downstream Mach number, M_2, by expressing A_2 in terms of M_2, Eq. (5), and substituting the above values for M_1 and A_1. The results are plotted in Figs. 4 and 5. The

maximum value of M_2 is 1 because the velocity cannot exceed the local speed of sound in a constant-area flow.

As an example, we assume that P_1 = 50,000 Pa (0.5 atmosphere) and P_2 = 500 Pa (3.75 torr), so that $P_2/P_1 = 0.01$. Using Figs. 4 and 5, we obtain $M_2 = 0.3$, $T_2/T_1 = 0.98$, $V_2/V_1 = 100$, and $\rho_2/\rho_1 = 0.01$. Because V_1 = 1 m/s and T_1 =26°C, we find V_2 = 100 m/s and T_2 =20°C. This relatively high-velocity and low-temperature jet can cause uneven cooling of the hot coil and result in serious damage, despite some drop in velocity and increase in temperature in the jet after it enters the furnace.

The problem of uneven cooling was evident in fired coils whose front surfaces (i.e., the surface directly exposed to the cold-oxygen jet) retained their approximate original dimensions but whose rear surfaces were badly bloated. The problem can be partially alleviated by increasing the pressure ratio, either by reducing the upstream pressure, P_1, or increasing the downstream pressure, P_2. This will reduce the velocity of the jet stream, V_2; however, the temperature of the jet entering the furnace will still be much lower than that of the sample, and this can result in uneven cooling of the coil. Alternative solutions are to heat the gas before it enters the furnace, or place a porous ceramic material between the furnace entrance and the coil (Fig. 3). The second alternative solution serves two purposes: (a) the porous material forces the oxygen to flow along a tortuous path, thereby allowing the oxygen to heat up before it contacts the coil, and (b) the porous material gives a more uniform flow of oxygen through the furnace, rather than a single small jet of oxygen down its center.

Heat Conduction. During firing, heat is applied at the coil surface and conducted into its interior. Heating in this manner establishes a temperature gradient, whose magnitude depends on the heating rate and the size of the coil. Large temperature gradients should be avoided for two reasons: (a) they induce thermal stresses in a structurally weak body, (b) because decomposition of the organics occurs over a small temperature range (≈5–10°C) [8], large gradients can establish a situation in which part of the coil is undergoing organic removal while another part is not. This also leads to stresses in the weak green body. To understand the effects of heating rate and sample size, the one-dimensional heat-conduction equation was solved for a surface temperature that increases linearly with time.

The assumed geometry for the analysis is shown in Fig. 6. A slab with thickness 2b is initially at a uniform temperature, T_o, and the surface temperature is increased linearly with time. In the figure, x = 0 corresponds to the center of the slab. The one-dimensional, transient heat-conduction equation is

$$\frac{\partial T}{\partial t} = \alpha \frac{\partial^2 T}{\partial x^2}, \tag{9}$$

where α is the thermal diffusivity of the sample. The initial condition is

$$t = 0,\ T = T_o\ , \tag{10}$$

and the boundary conditions are

$$x = \pm b,\ T = T_o + at, \tag{11}$$

where a is a constant that can be considered the heating rate (°C per unit time). The solution in terms of dimensionless parameters is given by [11]

$$T^* = t^* + \frac{x^{*2}-1}{2} + \frac{16}{\pi^3}\sum_{n=o}^{\infty}\frac{(-1)^n}{(2n+1)^3}\exp\left[\frac{-(2n+1)^2\pi^2 t^*}{4}\right]\cos\frac{(2n+1)\pi x^*}{2}, \tag{12}$$

where

$$T^* = \alpha(T-T_o)/ab^2, \tag{13}$$

$$t^* = \alpha t/b^2, \tag{14}$$

and

$$x^* = x/b. \tag{15}$$

The results from solving Eq. (12) are shown in Fig. 7. Because the temperature at the surface increases constantly with time, it increases with time everywhere in the sample. Also, the temperature increase at the interior always lags behind that at the surface, so that a temperature gradient exists at all times. The variations of the surface and centerline temperatures are plotted versus time in Fig. 8, where we see that the temperature gradient between the surface and the centerline approaches a constant value for $t^* > 1$. For large t^*, the exponential term in Eq. (12) becomes very small and

$$T^* = t^* + (x^{*2} - 1)/2. \tag{16}$$

Then,

$$\text{Surface } T^* = T^*(x^* = 1) = t^* \tag{17}$$

and

$$\text{Centerline } T^* = T^*(x^* = 0) = t^* - 0.5. \tag{18}$$

Therefore,

$$\text{Surface } T^* - \text{Centerline } T^* = 0.5. \tag{19}$$

This agrees with the result shown in Fig. 8 for large values of t^*.

If the thermal diffusivity of the sample is known, the steady-state temperature gradient (i.e., for large t^*) can be estimated from Eq. (19). The thermal diffusivity of the coil depends on the thermal diffusivities and volume fractions of all coil constituents. In the green state, coils consist of ceramic and silver powder embedded in a matrix of organic constituents. Because the YBCO and silver comprise such a low volume fraction of the green coil and the organics form a continuous phase, the thermal conductivity will be on the order of that for the organic constituents. Assuming the thermal diffusivity of the organic phase to be that of the acrylic binder (because it is the major component), the thermal diffusivity is estimated to be in the range of 10^{-7}-10^{-8} m^2/s [12,13].

Figure 9 shows the steady-state temperature gradient calculated for various sample thicknesses, assuming a value of 10^{-8} m^2/s for the thermal diffusivity. For example, if the thickness (2b) of the sample is ≈2 cm and the heating rate is 0.01°C/s, the temperature gradient between the surface and the centerline of the sample is ≈50°C. With such a large temperature gradient, the exterior of a coil can undergo organic decomposition and produce CO_2 while the organic phase in the coil interior remains intact. This type of situation is expected to impede the overall removal of organics and generate large stresses in the weak, green coil. In fact, coils fired at such a heating rate have disintegrated on numerous occasions. On the other

hand, a steady-state gradient of only ≈1°C is expected when thicker coils (2b ≈ 4 cm) are fired at the much slower heating rate of 6×10^{-4} °C/s. Coils fired at the slower heating rate have never bloated or exploded, possibly because the removal of organics proceeds in a more uniform fashion.

Heat conduction is also important to another crucial aspect of organic removal. Because the oxidation of binders is largely exothermic [14], it is critical that the heat generated during oxidation be efficiently removed; otherwise, thermal runaway at the interior can result in destruction of the green body. To estimate the conditions under which thermal runaway might be expected, the kinetics of binder decomposition must be known. As this information is not known at this time, we have not analyzed this aspect of organic removal.

Diffusion of Volatile Components. During the early, low-temperature stage of binder removal (below ≈200°C), volatile components of the organic phase are removed from the surface of the sample by evaporation. This evaporation of the volatile organics creates porosity in the green body and thereby facilitates removal of the binder at higher temperatures. If the binder remains in solid form at these low temperatures, migration of the volatile components to the surface proceeds by the slow process of diffusion. If the organics at the interior of the coil volatilize much more rapidly than they diffuse to the surface, bubbles can form and result in bloating of the coil. For this reason, it is important to consider diffusion of the volatile organics to the surface.

The diffusion problem is mathematically similar to the problem of heat conduction described in the previous section. The governing equation for

diffusion is

$$\frac{\partial C}{\partial t} = \delta \frac{\partial^2 C}{\partial x^2}, \tag{20}$$

where C is the concentration of the volatile component and δ is its diffusion coefficient through the binder. Again, we base our analysis on the geometry shown in Fig. 6, and use the following initial and boundary conditions:

$$t = 0,\ C = C_o \tag{21}$$

$$\frac{\partial C}{\partial x} = 0, \tag{22}$$

$$x = b;\ C = C_{surf}, \tag{23}$$

where C_o is the initial concentration of the volatile organic, and C_{surf} is its concentration at the surface of the coil. The surface concentration will be very small if the rate of evaporation is much larger than the rate of diffusion to the surface. The solution in terms of the dimensionless concentration C* is

$$C^* = 1 - \frac{4}{\pi} \sum_{n=o}^{\infty} \frac{(-1)^n}{(2n+1)} \exp\left[\frac{-(2n+1)^2 \pi^2\, t^*}{4}\right] \cos \frac{(2n+1)\pi x^*}{2}, \tag{24}$$

where

$$C^* = (C - C_o)/(C_{surf} - C_o), \tag{25}$$

$$t^* = \delta t/b^2, \tag{26}$$

and

$$x^* = x/b. \tag{27}$$

Based on Eqs. (24)-(27), Fig. 10 shows the dimensionless concentration as a function of position in the sample for various values of dimensionless

time, and Fig. 11 shows the centerline concentration as a function of dimensionless time. We see from Fig. 11 that for $t^* = 1.0$,

$$\text{Centerline } C^* = 0.90 = (C_{cent} - C_o)/(C_{surf} - C_o). \tag{28}$$

Because the evaporation rate is likely to be much greater than the diffusion rate, the surface concentration is negligible ($C_{surf} \approx 0$), and the centerline concentration turns out to be,

$$C_{cent} = 0.10C_o. \tag{29}$$

Thus, $t^* = 1.0$ corresponds to the time required for the centerline concentration to decrease to 10% of its initial value. Equation (26) shows that this time is a function of the thickness of the sample and the diffusion coefficient.

Very few data exist on the diffusion coefficient of volatile components in polymeric materials such as binders. Recently reported data on the diffusion coefficient of dialkyl phthalates in polyvinyl butyral [15] ranged from

$$\delta = 10^{-14} \text{ to } 10^{-16} \text{ m}^2/\text{s} \tag{30}$$

in the temperature range of 60–150°C. These values for the diffusion coefficient are several orders of magnitude smaller than the thermal diffusivity. If we use $t^* = 1.0$ as a measure of the characteristic time required for heat and mass transfer, it can be inferred that the time required for the diffusion of volatile components to the surface is much longer than that required for heat to be conducted to the interior of the sample. This indicates that the entire sample may be above the saturation temperature while most of the volatile components are still trapped in the

interior of the binder. Consequently, boiling may occur in the interior of the sample and cause the formation of bubbles. Bubble formation during binder burnout has been experimentally observed and is considered a likely source of defects in the fired body [16]. To alleviate this problem, the heating rate should be kept low, and enough time must be provided to accommodate the slow process of diffusion.

Conclusions

The removal of organics is a complicated process that involves both heat and mass transfer through a structurally weak body and is critical in fabricating superconductors by methods that involve large amounts of organics. To better understand and control the removal of organics from YBCO coils, the following variables of heat treatment were considered: total pressure in the furnace, oxygen flow, heat conduction, and diffusion of volatile components.

Firing coils at reduced pressure was found to greatly minimize, if not eliminate, decomposition of YBCO for two possible reasons: (a) CO_2 and H_2O are not allowed to accumulate in the atmosphere because the furnace operates under a dynamic vacuum, thus minimizing the reaction between YBCO and CO_2 and H_2O, (b) the reduced pressure limits the supply of oxygen to the decomposing binder, thereby moderating the binder decomposition reaction and preventing thermal runaway. It was also shown that uneven cooling of the coil can result if oxygen is allowed to flow unimpeded into the furnace. Disrupting the flow of oxygen by placing a porous material at the entrance to the furnace helps to alleviate this problem.

Heat conduction into the coil interior is controlled by the thermal diffusivity of the organic phase. Because this thermal diffusivity is very low (10^{-7}–10^{-8} m^2/s), large steady-state temperature gradients (≈50°C) might be expected across moderately thick coils (≈2 cm) that are heated at rates of ≈0.01°C/s. This can lead to nonuniform removal of organics from the coil and result in large stresses in the weak green coil. Calculations and experiments show that this problem is avoided when coils are heated at a rate of ≈0.001°C/s. Finally, it was shown that the diffusion of volatile components is much slower than heat conduction, so the entire coil may be above the saturation temperature while most of the volatile components are still trapped in the interior. This results in bubble formation and can be prevented by the use of very slow heating rates.

Acknowledgments

Work was supported by the U.S. Department of Energy, Conservation and Renewable Energy, as part of a program to develop electric power technology, under Contract W-31-109-Eng-38.

References

1. T. Nakahara, Proc. World Congress on Superconductivity, Houston, TX, pp. 88–103, World Scientific Press, Teaneck, NJ, 1988.

2. P. K. Gallagher, G. S. Grader, and H. M. O'Bryan, Mat. Res. Bull., 23, 1491 (1988).

3. E. K. Chang, E. F. Ezell, and M. J. Kirschner, Supercond. Sci. Technol., 8, 391 (1990).

4. T. B. Lindemer, C. R. Hubbard, and J. Brynestad, Physica C., 167, 312 (1990).

5. T. M. Shaw, D. Dimos, P. E. Batson, A. G. Schrott, D. R. Clarke, and P. R. Duncombe, J. Mater. Res., 5, 1176 (1990).

6. Y. Gao, K. L. Merkle, C. Zhang, U. Balachandran, and R. B. Poeppel, J. Mater. Res., 5, 1363 (1990).

7. Y. Gao, Y. Li, K. L. Merkle, J. N. Mundy, C. Zhang, U. Balachandran, and R. B. Poeppel, Mater. Lett., 9, 347 (1990).

8. S. E. Dorris, J. T. Dusek, J. J. Picciolo, R. Russell, J. P. Singh, and R. B. Poeppel, Proceedings of the Intl. Conf. on Electric Machines (ICEM), Cambridge, MA, Aug. 12-15, 1990.

9. W. Wong-Ng, R. S. Roth, L. J. Schwartzendruber, L. H. Bennett, C. K. Chiang, F. Beech, C. R. Hubbard, Adv. Ceram. Mater., 2, 565 (1987).

10. A. H. Shapiro, The Dynamics and Thermodynamics of Compressible Fluid Flow, Vol. 1, The Ronald Press Company, New York, 1953.

11. H. S. Carslaw and J. C. Jaeger, Conduction of Heat in Solids, 2nd Edition, Oxford University Press, 1959.

12. Polymer Handbook, Edited by J. Brandrup and E. H. Immergut, 2nd Edition, John Wiley & Sons, New York, 1975.

13. W. J. Roff and J. R. Scott, Fibres, Films, Plastics, and Rubbers, A Handbook of Common Polymers, Butterworth & Co. Ltd., 1971.

14. V. N. Shukla and D. C. Hill, J. Am. Ceram. Soc., 72(10), 1797 (1989).

15. J. A. Lewis and M. J. Cima, J. Am. Ceram. Soc., 73(9), 2702 (1990).

16. C. Dong and H. K. Bowen, J. Am. Ceram. Soc., 72(6), 1082 (1989).

Table 1. Description and Properties of Six Superconductor Coils and Their Firing Conditions

Coil Description	Firing Conditions	J_c (A/cm^2)	B (Air Core)[a] (Gauss)	B (Fe Core)[b] (Gauss)
1. Uncoated 25 Turns	100% O_2 910°C	120	19	–
2. 211–Coated 25 Turns	100% O_2 910°C	130	20	–
3. Uncoated 21 Turns	2 mm Hg 875°C	225	36	–
4. 211–Coated 2 Layers 42 Turns	10 mm Hg 875°C	150	42	160 @ 77 K
5. 211–Coated 5 Layers 72 Turns	10 mm Hg 875°C	150	73	330 @ 77 K 420 @ 73 K
6. 211–Coated 6 Layers 120 Turns	10 mm Hg 900°C	140	80	–

[a]Magnetic field generated at center of coil when coil was operating just below its critical current.

[b]Magnetic field generated across an ≈6-mm gap for an iron core.

FIGURE CAPTIONS

Fig. 1. Schematic X-ray patterns of fully oxygenated YBCO powders and two other YBCO powders that were fired at ambient pressure in contact with the organics used in extrusion. The patterns show that both powders fired with the organics decomposed during firing.

Fig. 2. Schematic X-ray patterns of YBCO powder as a function of temperature. The powder was fired at reduced total pressure in contact with organics used in extrusion, and showed no signs of decomposition.

Fig. 3. Schematic diagram of the furnace used to fire coils.

Fig. 4. The ratios of pressure, P_2/P_1, and temperature, T_2/T_1, at Points 1 and 2, plotted as functions of the downstream Mach number, M_2.

Fig. 5. The ratios of gas velocity, V_2/V_1, and density, ρ_2/ρ_1, at Points 1 and 2, plotted as functions of the downstream Mach number, M_2.

Fig. 6. The idealized, one-dimensional geometry on which the analyses of heat conduction and diffusion of volatile components are based.

Fig. 7. The dimensionless temperature, T^*, as a function of dimensionless position, x^*, in the idealized sample, plotted for various values of dimensionless time, t^*.

Fig. 8. The dimensionless temperature at the center of the sample, T^*, as a function of dimensionless time, t^*.

Fig. 9. The temperature gradient across the sample as a function of dimensionless time, t^*.

Fig. 10. The dimensionless concentration, C^*, as a function of dimensionless position, x^*, for various values of dimensionless time, t^*.

Fig. 11. The dimensionless concentration at the center of the sample versus dimensionless time, t^*.

Nomenclature

A: Constant defined by specific heat ratio and Mach number. See Eqn. 5.

C^*: Dimensionless concentration defined in Eqns. 24 and 25

C_1: Constant defined by specific heat ratio. See Eqn. 6.

M_1, M_2: Mach number at points 1 and 2 in experimental setup

P_1, P_2: Total pressure at points 1 and 2 in experimental setup

t: time

t^*: Dimensionless time defined in Eqn. 14 for heat conduction, in Eqn. 26 for diffusion of volatile components

T_1, T_2: Temperature at points 1 and 2 in experimental setup

V_1, V_2: Gas velocity at points 1 and 2 in experimental setup

x: Position in idealized sample

x^*: Dimensionless position defined in Eqn. 15

α: Thermal diffusivity

δ: Diffusion coefficient

γ: Specific heat ratio

ρ_1, ρ_2: Gas density at points 1 and 2 in experimental setup

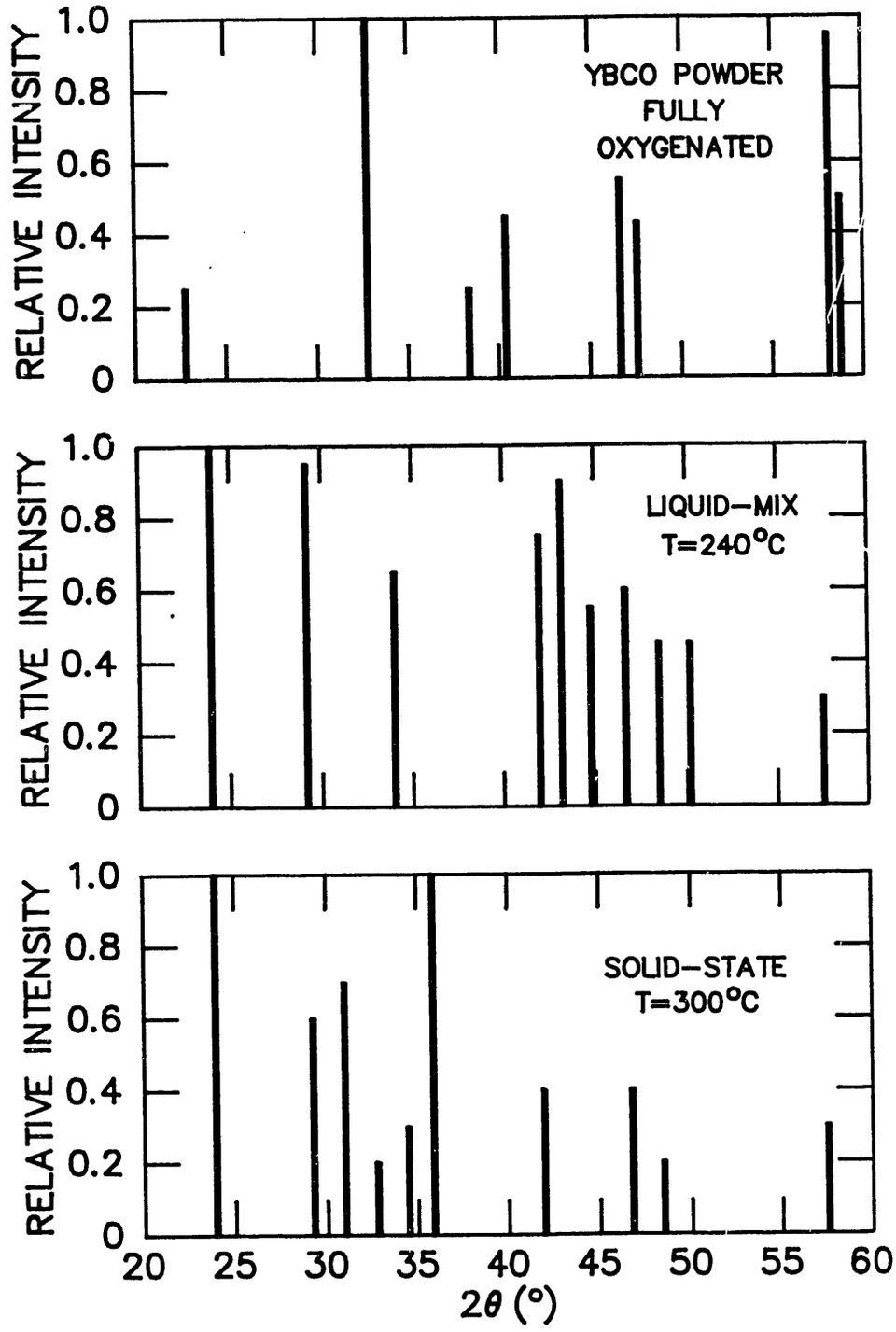

Fig. 1. Schematic X-ray patterns of fully oxygenated YBCO powders and two other YBCO powders that were fired at ambient pressure in contact with the organics used in extrusion. The patterns show that both powders fired with the organics decomposed during firing.

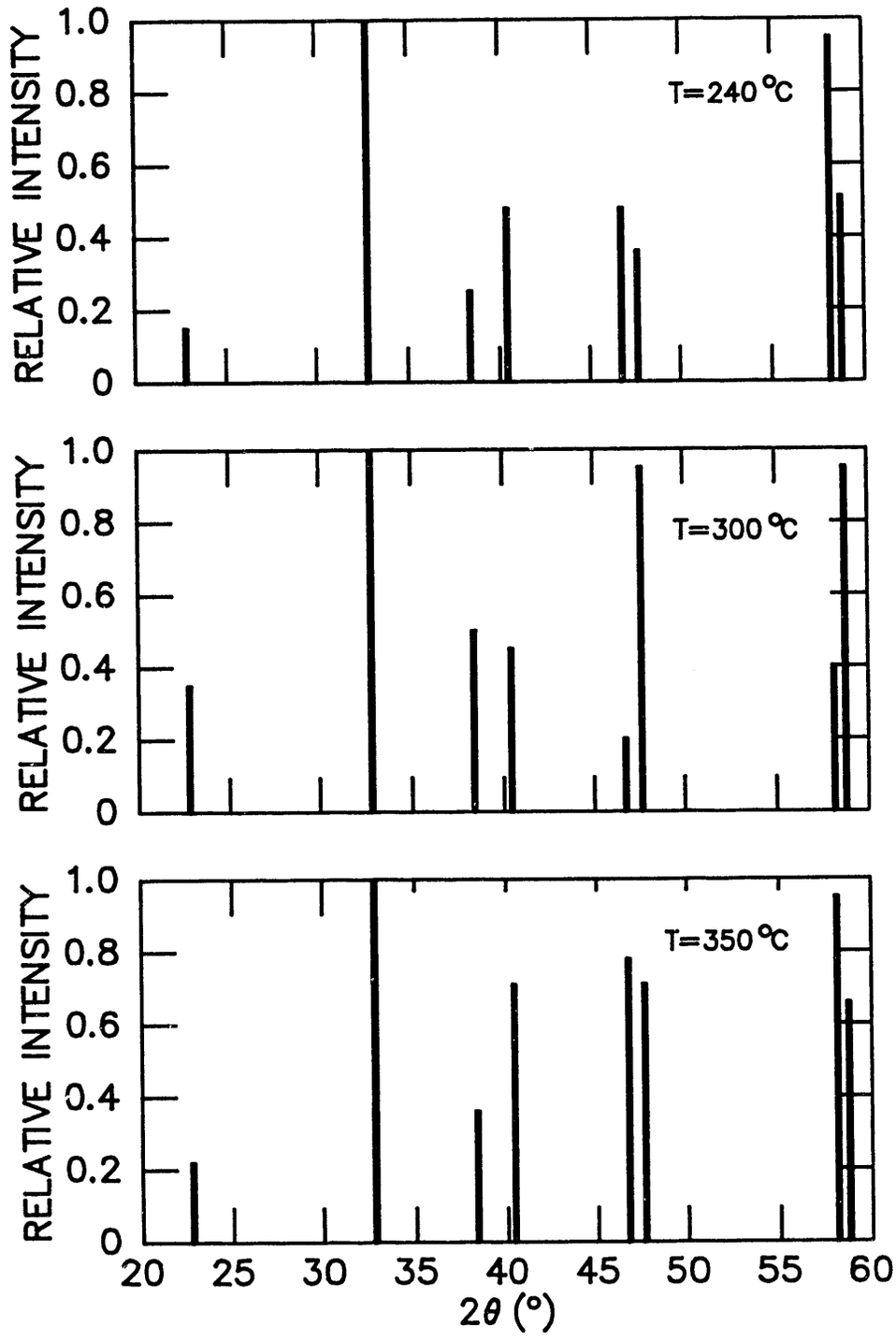

Fig. 2. Schematic X-ray patterns of YBCO powder as a function of temperature. The powder was fired at reduced total pressure in contact with the organics used in extrusion, and showed no signs of decomposition.

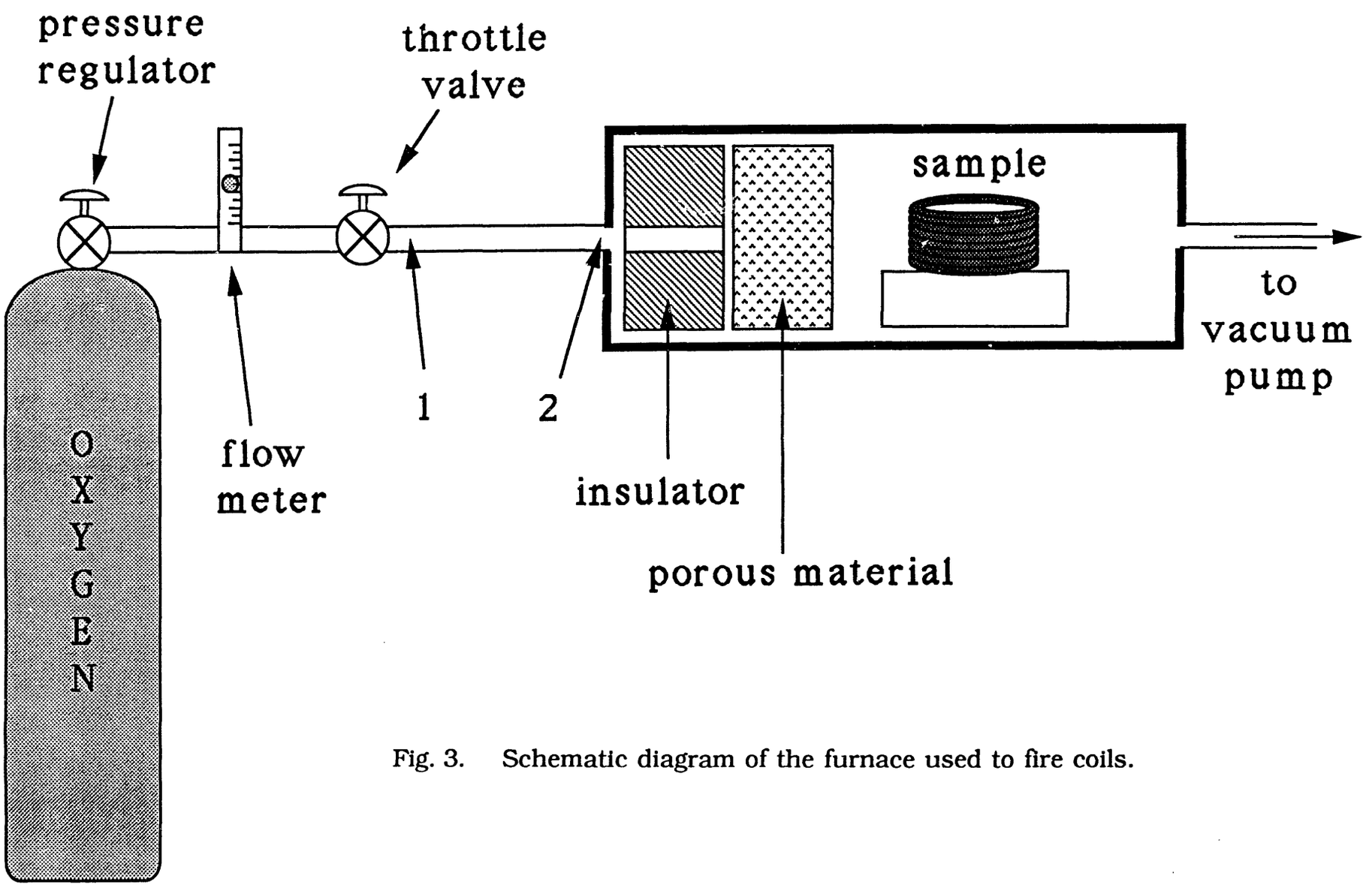

Fig. 3. Schematic diagram of the furnace used to fire coils.

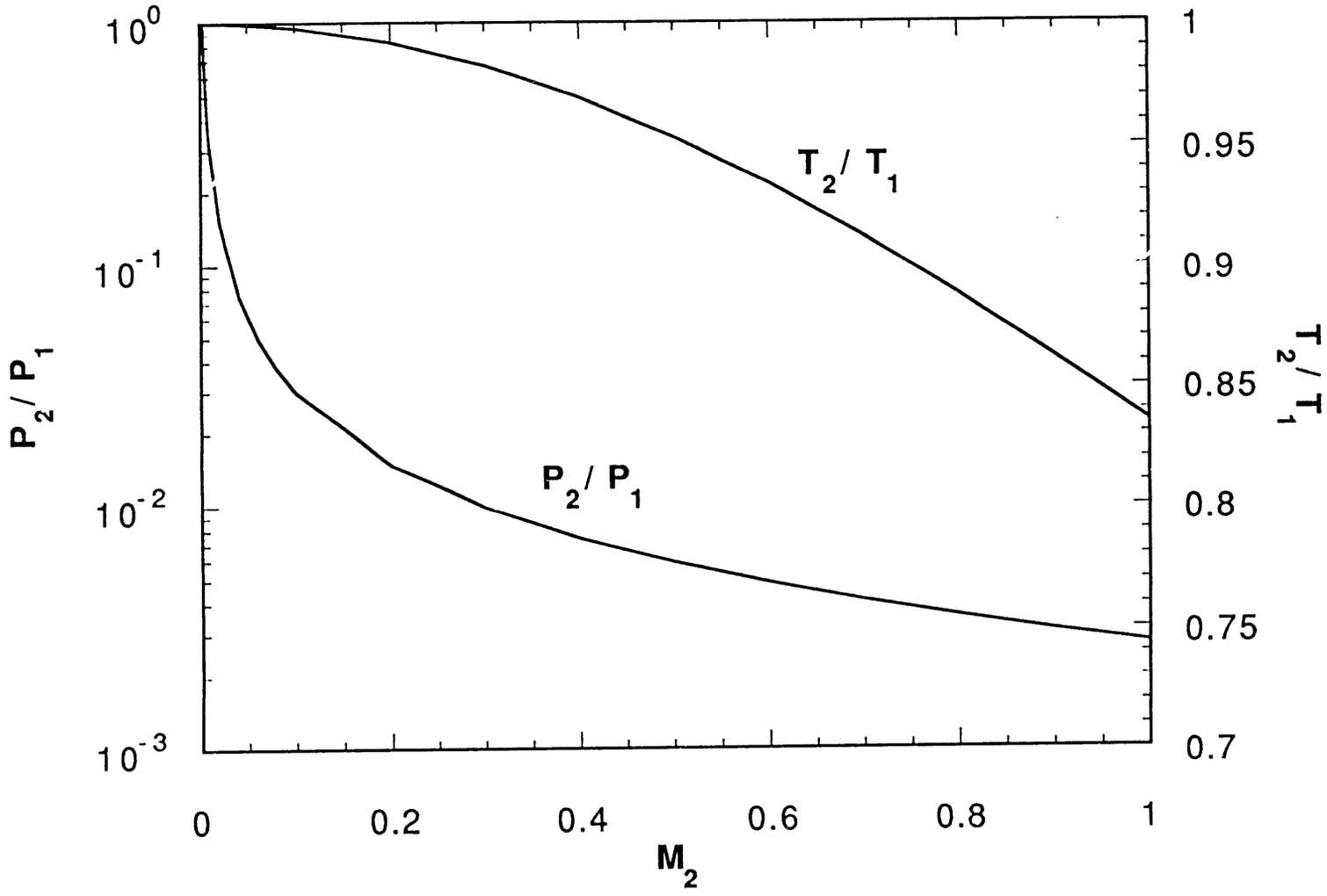

Fig. 4. The ratios of pressure, P_2/P_1, and temperature, T_2/T_1, at Points 1 and 2, plotted as functions of the downstream Mach number, M_2.

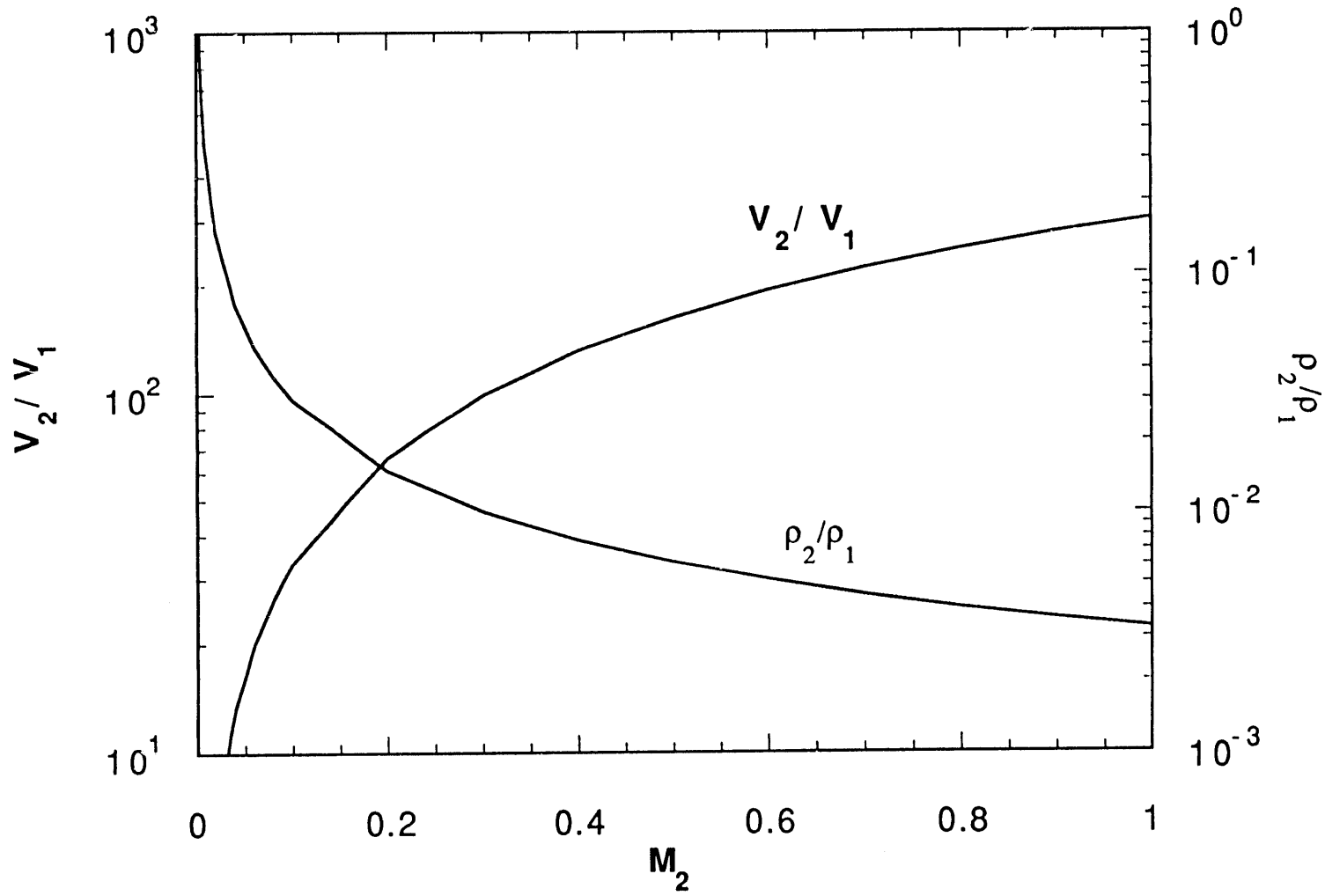

Fig. 5. The ratios of gas velocity, V_2/V_1, and density, ρ_2/ρ_1, at Points 1 and 2, plotted as functions of the downstream Mach number, M_2.

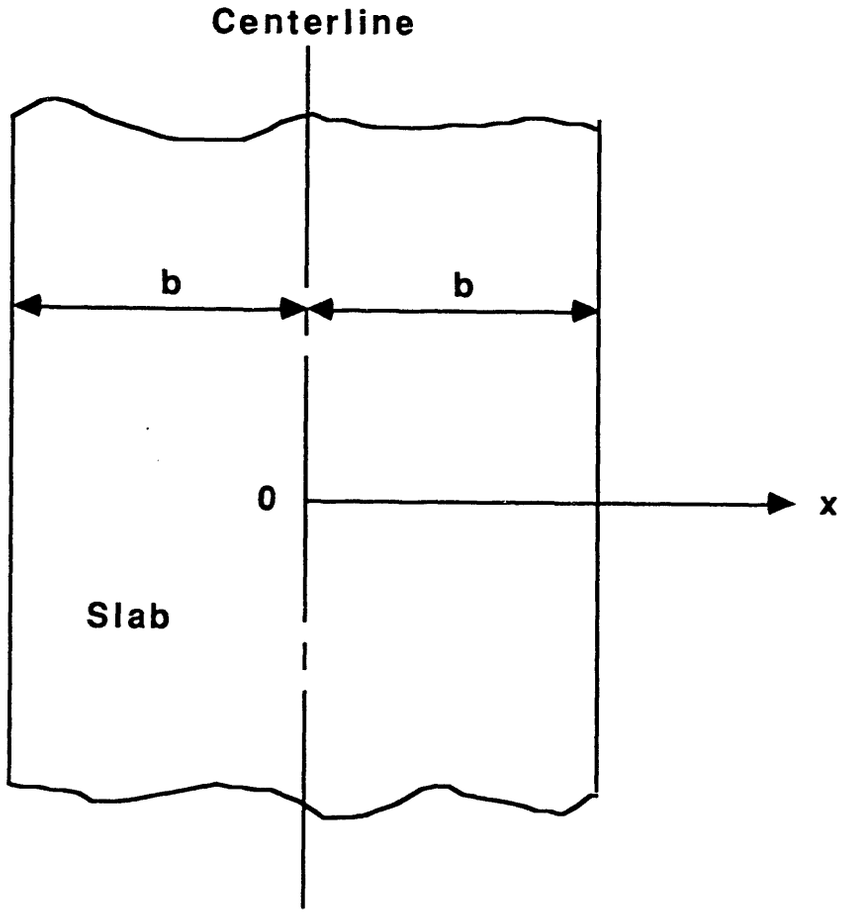

Fig. 6. The idealized, one–dimensional geometry on which the analyses of heat conduction and diffusion of volatile components are based.

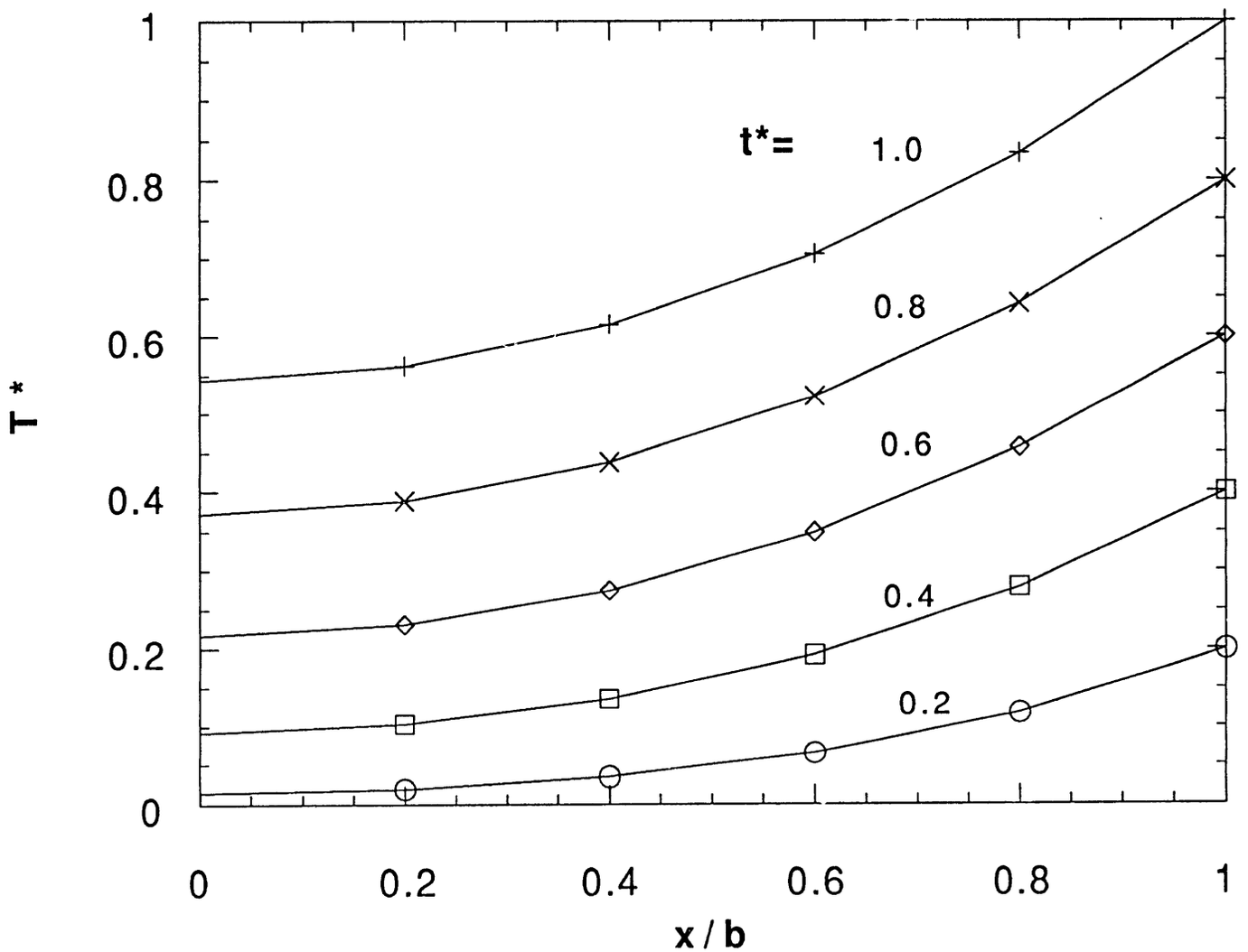

Fig. 7. The dimensionless temperature, T^*, as a function of dimensionless position, x^*, in the idealized sample, plotted for various values of dimensionless time, t^*.

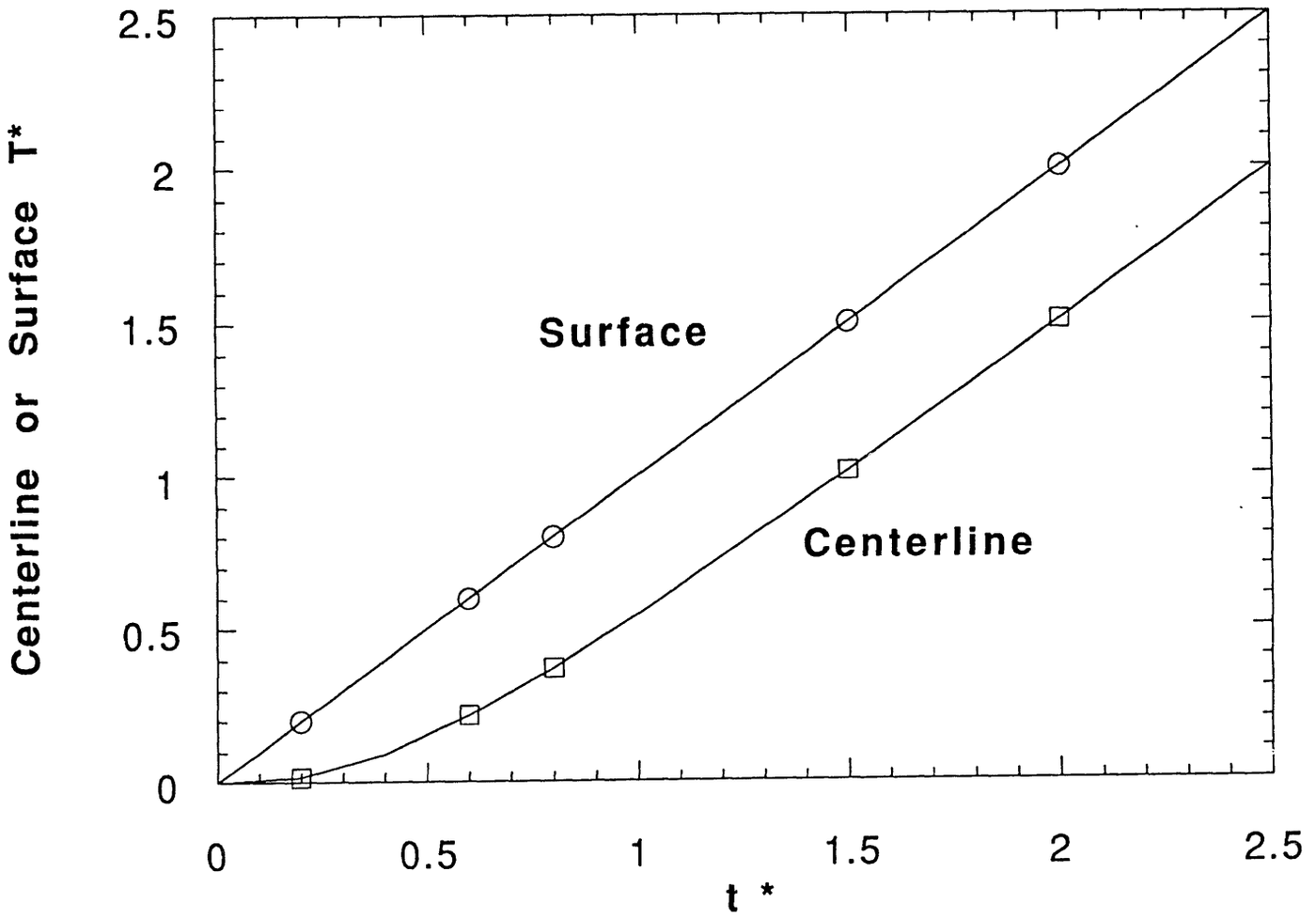

Fig. 8. The dimensionless temperature at the center of the sample, T^*, as a function of dimensionless time, t^*.

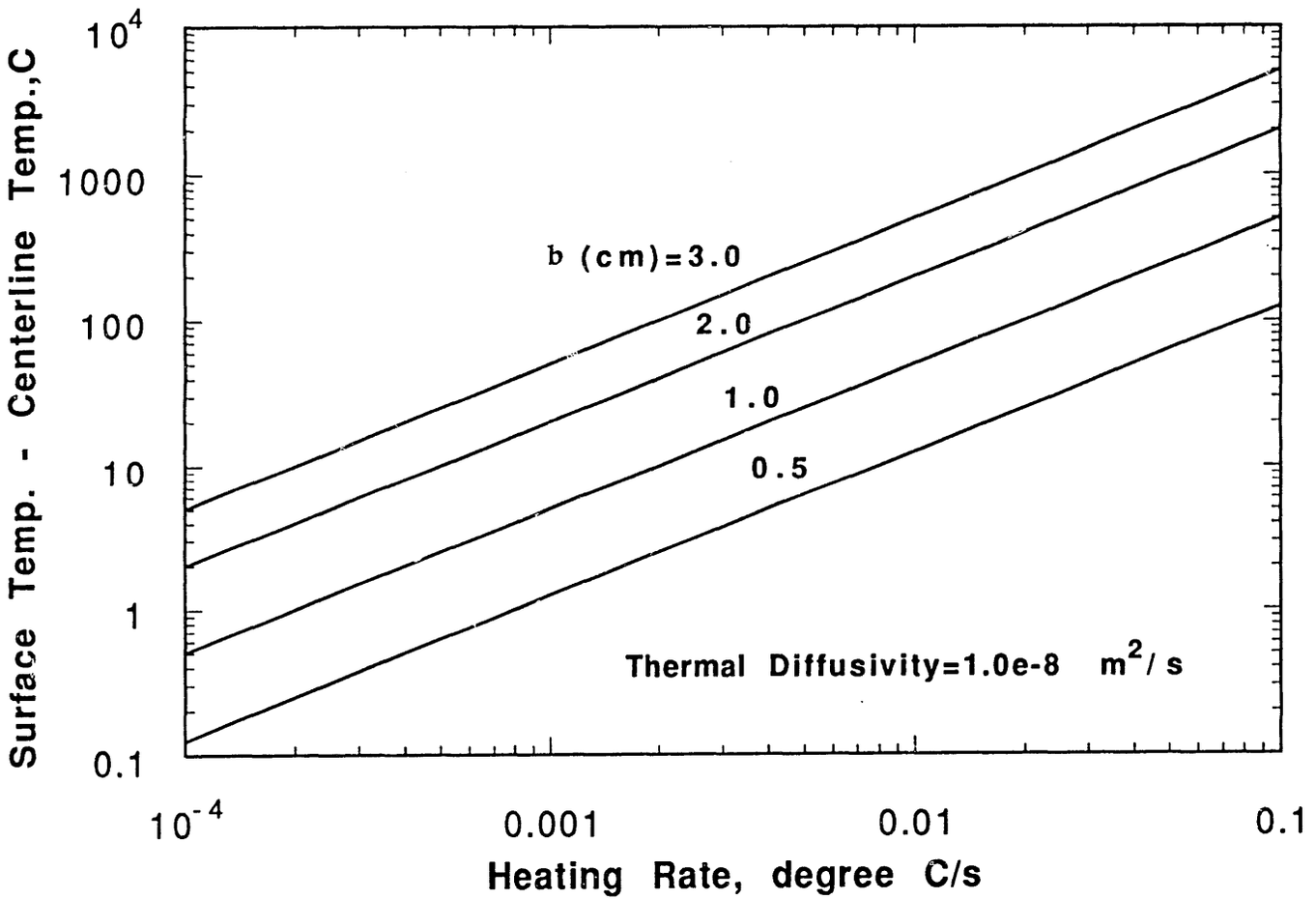

Fig. 9. The temperature gradient across the sample as a function of the dimensionless time, t^*.

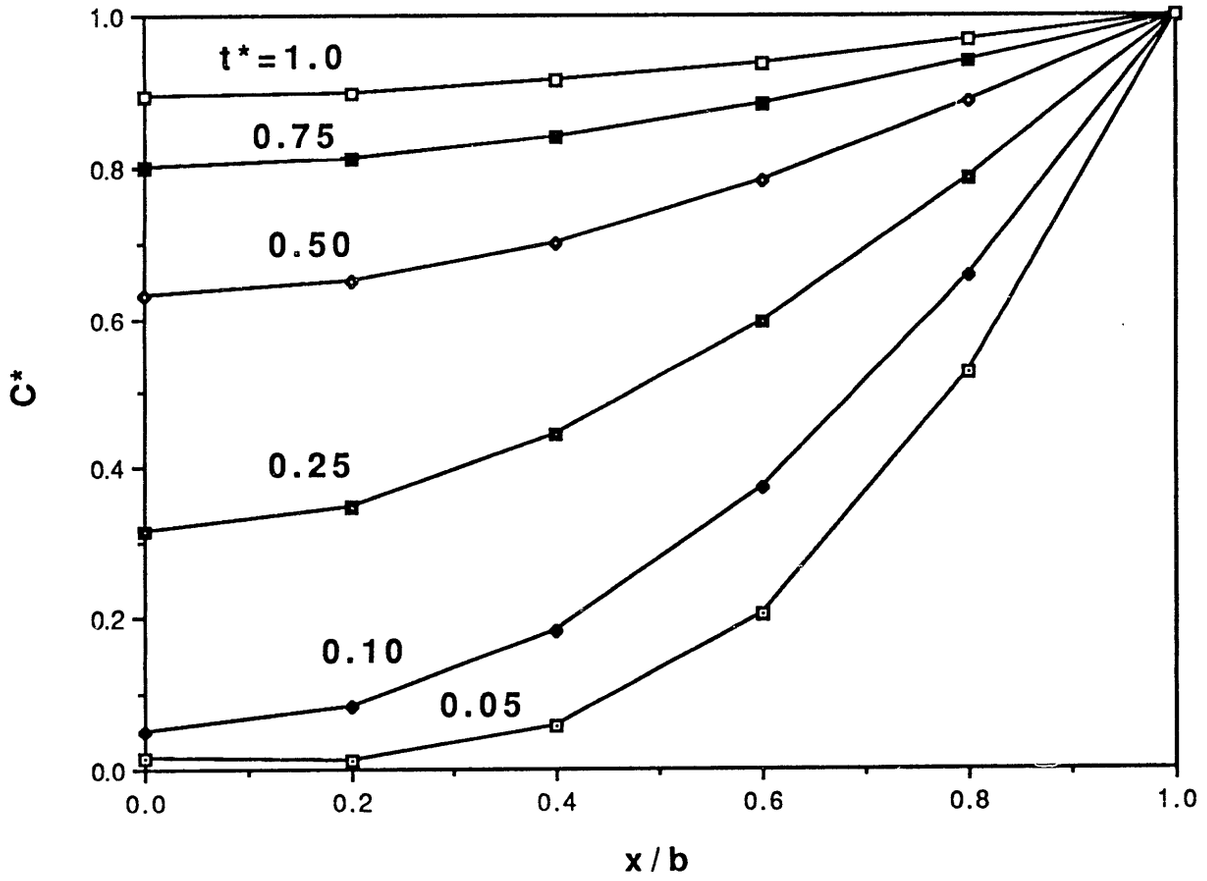

Fig. 10. The dimensionless concentration, C^*, as a function of dimensionless position, x^*, for various values of dimensionless time, t^*.

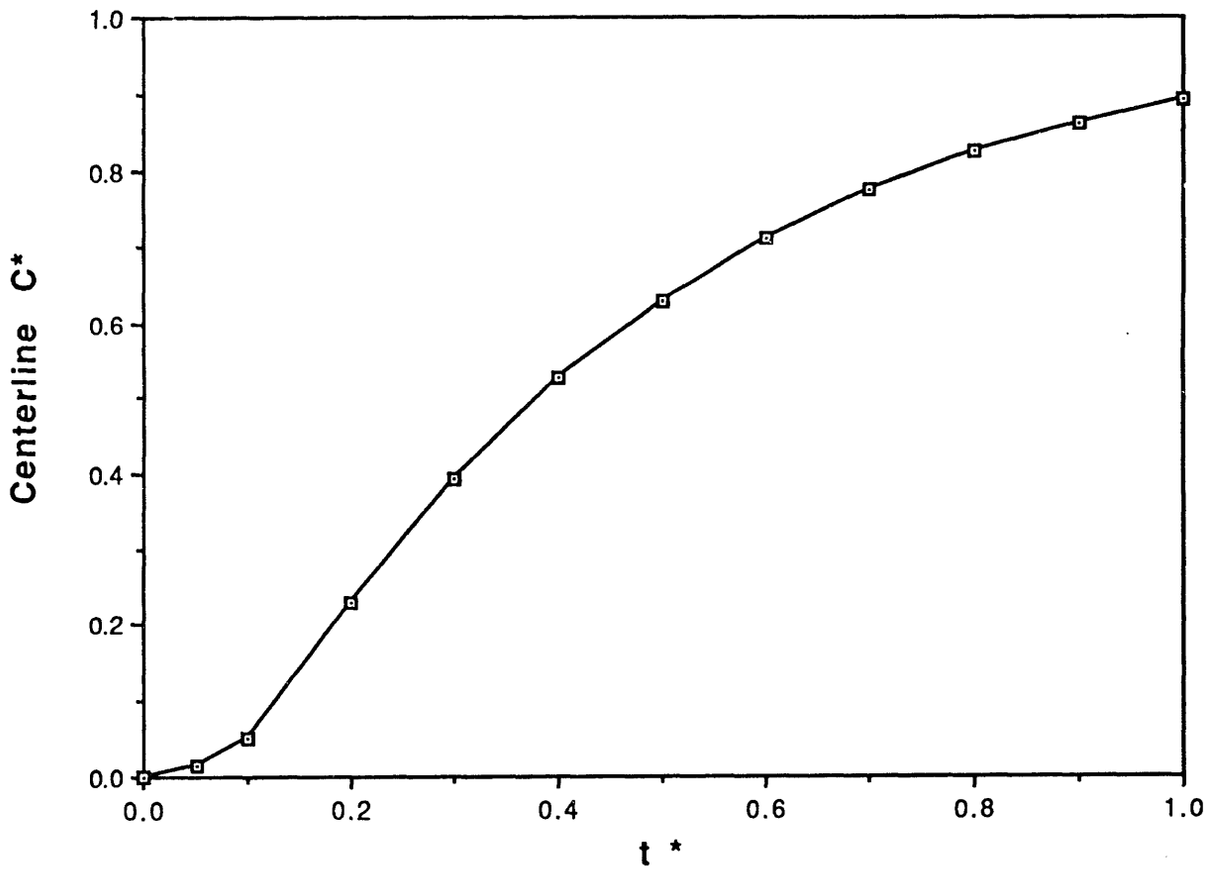

Fig. 11. The dimensionless concentration at the center of the sample versus dimensionless time, t^*.

END

DATE FILMED

01/24/92